



1

1

2

3

Seasonal cycle in surface seawater isotopic composition

4

5

6

7 Gilles Reverdin¹, Claire Waelbroeck¹, Lola Goeme¹, Antje H. L. Voelker^{2,3}, Hans-Christian
8 Steen-Larsen⁴

9

10

11

12 ¹ Laboratoire LOCEAN/IPSL, Sorbonne Université-CNRS-IRD-MNHN, Paris, 75005,
13 France

14 ² Instituto Português do Mar e da Atmosfera (IPMA), Algés, Portugal

15 ³ Center of Marine Sciences (CCMAR), Universidade do Algarve, Faro, Portugal

16 ⁴ Geophys. Inst., Univ. Bergen, Bergen, Norway

17

18 Corresponding author: Gilles Reverdin gilles.reverdin@locean.ipsl.fr

19



2

20 Abstract

21 Data of stable isotopologs of water in the quality-controlled CISE-LOCEAN database provide
22 an unprecedented sampling of the surface Atlantic Ocean and the southwest Indian Ocean.
23 This investigation of $\delta^{18}\text{O}$, $\delta^2\text{H}$ and deuterium excess (d-excess) in surface sea water
24 indicates large variability of the regional regression lines with salinity as a function of
25 latitude for $\delta^{18}\text{O}$ and $\delta^2\text{H}$, with weakest slopes near equator, but also to a lesser extent
26 with weaker slopes in the western Atlantic compared with the eastern Atlantic at low
27 and mid-latitudes. These regressions often explain a large share of the variability in the
28 data (40 to 70%), except for d-excess at the higher latitudes and $\delta^{18}\text{O}$, $\delta^2\text{H}$ near the
29 equator. The data are sufficient to extract a seasonal variability in these relationships
30 and an average seasonal cycle in some regions of the North Atlantic subpolar gyre with
31 signals probably related to changes in the input of heavier sea ice melt and depleted
32 water of Arctic origin. A seasonal cycle is also found in the central equatorial Atlantic
33 with the strong contrast between the vicinity of the equator and the region to its north,
34 associated with the seasonal shift of the precipitation belt and with the seasonality of
35 the equatorial upwelling. In those regions there is also some evidence in seasonal
36 variability of the d-excess that is not currently explained. Elsewhere, the seasonal signal
37 usually does not come out of the noise. A 7-8 years long time series of nearly monthly
38 surface sampling at the BATS site near Bermuda (31°50'N, 64°10'W) also indicates a
39 rather well-defined seasonal cycle of SSS, $\delta^{18}\text{O}$, $\delta^2\text{H}$ and deuterium excess. There is also
40 some indication of interannual variability, which might not be closely related to salinity.



3

41

42 1. Introduction

43 Seawater isotopic composition ($^{18}\text{O}/^{16}\text{O}$ and $^2\text{H}/^1\text{H}$ ratios expressed as $\delta^{18}\text{O}$ and $\delta^2\text{H}$ in
44 ‰ (per mille) in the VSMOW/SLAP scale) is classified as an Essential Ocean/Climate
45 Variable (EOV/ECV) in international programs such as GEOTRACES and GO-SHIP. These
46 stable seawater isotopes are used to trace sources of freshwater (precipitation,
47 evaporation, runoff, melting glaciers, sea ice formation and melting), both at the ocean
48 surface and in the ocean interior (Schmidt et al., 2007; Hilaire-Marcel et al., 2021).

49 A major emphasis in the data collection has been on the high latitude oceans. There,
50 continental (or icebergs) glacial melt, formation or melt of sea ice, and high-latitude
51 river inputs (for the Arctic) leave imprints on the surface ocean isotopic composition,
52 and for the Southern Ocean in the top 800 m water column close to ice shelves (Hennig
53 et al., 2024). Seawater isotopes in the upper ocean at low latitudes are often vital for
54 paleoclimatic studies, as they are needed, often at a seasonal resolution, to calibrate
55 proxies of past ocean variability in marine carbonate records such as corals and
56 foraminifera (e.g., PAGES CoralHydro2k working group; Konecky et al., 2020, Atwood et
57 al., 2025). Additionally, surface ocean seawater isotopes are also used to characterize
58 evaporation rates and air-sea interactions (Benetti et al., 2017a).

59 Except for fractionation during phase changes, thus mostly at the sea surface, the water
60 isotopic composition is nearly conservative in the ocean, with chemical and biological
61 processes having minimal effect. Because of that, there tends to be quasi-linear
62 relationships between ocean salinity S (practical salinity with no unit) and water isotope
63 properties ($\delta^{18}\text{O}$, $\delta^2\text{H}$, but also d -excess defined as $\delta^2\text{H} - 8 \cdot \delta^{18}\text{O}$, together later referred
64 to as δ -isotopes), as exemplified for $\delta^{18}\text{O}$ in Legrande et al. (2006). In their paper,
65 regional relationships are used to reconstruct global distribution of water isotopes in
66 the surface ocean, as well as through the water column in order to provide a climatology
67 to which isotope-enabled models can be referred to. Regional relationships are also used
68 to characterize water masses or different freshwater sources during their formation
69 (Frew et al., 2000; Voelker et al., 2015).



4

70 Regional relationships are further used in Reverdin et al (2025) to identify systematic
71 biases between different data sets collected in the same years, but not necessarily in the
72 same season. That study, as well as Glaubke et al. (2024) also show how the
73 relationships between salinity and $\delta^{18}\text{O}$, $\delta^2\text{H}$, or d-excess vary spatially across the south
74 subtropical Indian Ocean, an indication of the possible limitation of the concept. Similar
75 spatial variability was also suggested across the North Atlantic subtropics in Benetti et
76 al (2017a).

77 At high latitudes, sampling primarily occurs during the summer, while at low latitudes,
78 data is more spread out throughout the year, but remains quite scarce. As a result, there
79 are relatively few low latitude regions with enough data to accurately estimate seasonal
80 variability (Atwood et al, 2025). Additionally, Atwood et al (2025) assume that there are
81 no remaining biases in the data sets and that interannual/decadal variability is minimal
82 or can be modelled. However, often, different relationships were found in nearby
83 regions between water isotopes and salinity that were sampled in different seasons,
84 such as the western and eastern North Atlantic subtropics in Benetti et al. (2017a),
85 which raises the question as whether these different differences are artifacts caused by
86 unresolved seasonal or interannual signals.

87 Fortunately, there have been some concerted attempts to resolve surface seasonal
88 variability, away from coastal areas. This has been the case, for example, since late 2010,
89 in the surface North Atlantic subpolar gyre (NASPG) between Iceland and North America
90 (Reverdin et al., 2018) extended more recently between southeastern Greenland and the
91 North Sea. A subset of these data was used in Benetti et al. (2014) to identify seasonal
92 variability of the relationship between water isotopes and salinity. These authors found
93 seasonal changes on the Labrador and Newfoundland shelves and close to them in the
94 western NASPG that were attributed to the cycle of sea ice formation in winter and sea
95 ice melt in spring, often upstream of the site of data collection. In the subtropics, a
96 concerted effort was also undertaken at the BATS site near Bermuda to regularly sample
97 surface-water isotopes since 2011.

98 2. Data and Methods

99 2.1 Data



5

100 Stable seawater isotope data have been produced in the last fifty years by a variety of
101 methods. For example, most data compiled in the “GISS Global Seawater Oxygen-18
102 Database -V1.21” for stable seawater isotopes (LeGrande and Schmidt, 2006) originate
103 from Isotope-ratio Mass Spectrometry (IRMS). They were mostly measured by dual-inlet
104 technology (highest precision), whereas, since 2000, the continuous-flow method (lower
105 precision) became widespread for seawater isotope analysis. Since 2010, laser
106 spectroscopy, in particular cavity ring-down spectroscopy (CRDS) turned into another
107 commonly used method as it allows parallel measurement of $\delta^{18}\text{O}$ and $\delta^2\text{H}$, but with
108 often lower precision, at least early on (e.g., Voelker et al., 2015). As CRDS (and other
109 laser techniques) have been commonly used for seawater isotope analysis since 2010,
110 they contribute a significant part of the data produced globally (see for example, the
111 compilation of the soon to be released CoralHydro2k seawater data base with a focus on
112 the tropics (35°N-35°S) (Atwood et al., 2025)).

113 There are potential differences between the data produced by the two methods,
114 discussed in Reverdin et al. (2022) in the context of the CISE-LOCEAN database. In this
115 database, part of the samples collected in 2010-2015 have been first distilled, whereas
116 more recent samples are directly introduced in the vaporizer associated with a Picarro
117 L2130 CRDS, through a salt-liner. For CRDS measurements, there are also issues of
118 memory effects due to the properties of water molecules to stick to the surfaces, and
119 more for $^1\text{H}^2\text{H}^{16}\text{O}$ than for the other isotopologs of the water molecule (cf fig. 4 of Steen-
120 Larsen and Zannoni, 2024). In this version of the database, these memory effects have
121 been roughly corrected based on inserting some reference material regularly (every
122 three seawater samples) with isotopic composition close to them, as well as by running
123 duplicates of samples at the beginning and end of each daily run, as well as of for
124 samples with large standard deviations between the different injections retained.

125 Furthermore, an attempt was made to adjust the data from these three measurement
126 methods (IRMS, CRDS with or without distillation), based on the analysis of Benetti et al
127 (2017b). Uncertainties are largest in the earlier IRMS measurements, because of
128 uncertainties on the reference material used at the time. As described in Reverdin et al
129 (2022), this was partially corrected based on deep water measurements measured at
130 the time, for which we expect little variability over the last 30 years. However, there
131 remains subsets of $\delta^{18}\text{O}$ data produced by IRMS which could not be fully assessed. This



6

132 is for example the case for surface samples collected in the equatorial Atlantic in August-
133 September 1998 and 1999. Compared with more recent data, they present a negative
134 $\delta^{18}\text{O}$ offset larger than -0.10% . This could be related to a calibration issue or
135 interannual variability. As there are no measurements for those years for the other
136 seasons or other isotopes, we have excluded those data when analyzing the summer
137 season in the equatorial Atlantic region. Interestingly, the slope of the regression of $\delta^{18}\text{O}$
138 with respect to salinity of these 1998-1999 data is consistent with the one of the more
139 recent data, thus suggesting similar processes involved in the spatial property
140 distribution in this earlier period.

141 There was also an attempt to identify and flag potential issues of evaporation of the
142 samples, happening mostly because of long storage in bottles which exchanged with the
143 outside air, or defective bottles or caps (Reverdin et al., 2022). Although these issues are
144 less common in the last 10 years of collected data, this still sometimes happens, in
145 particular with samples extracted from water bottles for salinity measurements
146 collected on Voluntary Observing Ships (VOS). Although these VOS data tend to present
147 less consistency, we retain them in the data base, because in some tropical-subtropical
148 areas, they contribute a significant share of the observations (Alory et al, 2015).

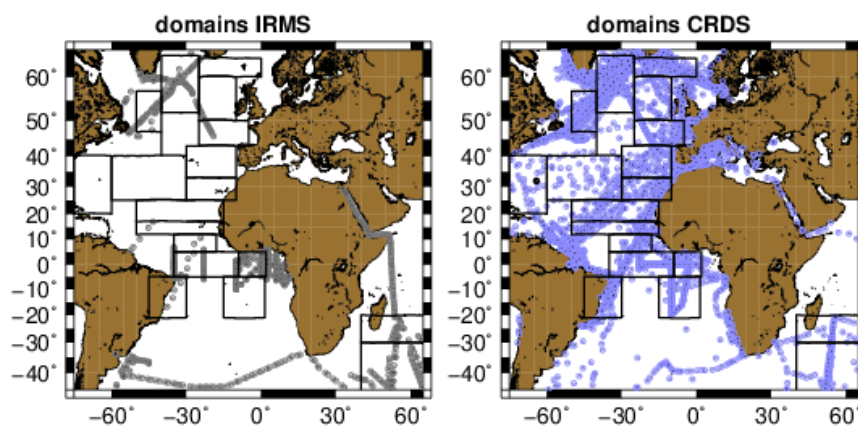
149 The validation steps, as well as the large percentage of surface data in the open ocean,
150 away from coasts in the CISE-LOCEAN data base (over 8200 validated $\delta^{18}\text{O}$ data
151 associated with a valid salinity since 1998) represent significant differences with
152 respect to other published data compilations such as the “GISS Global Seawater Oxygen-
153 18 Database -V1.21” for stable seawater isotopes which does not include the CISE-
154 LOCEAN data (LeGrande and Schmidt, 2006; referred to as GISS-V1.21), or the
155 CoralHydro2k seawater data base, which includes only part of the CISE-LOCEAN data
156 (Atwood et al., 2025). GISS-V1.21 is a compilation of different individual data sets
157 originating mostly from ocean cruises and measured by Isotope-ratio Mass
158 Spectrometry (IRMS), for which there was an attempt to correct systematic biases
159 between data subsets, and includes fewer surface data. The CoralHydro2k data base
160 does not offer systematic correction of potential biases between different datasets, but it
161 contains significant metadata that could be used for further evaluation. Furthermore,
162 the large proportion of surface data produced by CRDS in the LOCEAN data base (more
163 than 70% of the surface data) offers the opportunity to investigate $\delta^2\text{H}$ and d-excess, in



7

164 addition to $\delta^{18}\text{O}$, these two other variables been much less frequent in the GISS-V1-21
165 archive.

166 The sampling in the CISE-LOCEAN data base is heavily skewed to some subregions of the
167 ocean, such as the Atlantic Ocean and nearby seas, the south-western Indian Ocean and
168 between Tasmania and Antarctica. In some of these regions, there is usually some
169 seasonal sampling, albeit not much south of Tasmania, which will be ignored here, as
170 well as other world regions (Figure 1).



171

172 Figure 1: Maps of Wisotopes data distribution with the contours of the different domains
173 outlined. Left one for IRMS measurements, and right one for CRDS measurements. The
174 black dot in the western subtropical Atlantic on the left panel is at the BATS station site.

175 We also used surface samples collected mostly monthly at the BATS hydrographic site
176 near Bermuda (31°50'N, 64°10'W) in 2015-2022. These samples stored in plastic bottles
177 were frozen and stored at the University of Bergen before been analyzed in 2023 before
178 been refrozen. They were unfrozen in November 2025 to be transported to LOCEAN
179 where they were analyzed between December 5 2025 and January 11, but on a CRDS
180 unit which experienced a set of technical problems reducing the accuracy. There are also
181 indications that some of the samples had evaporated (five samples, in the Bergen
182 analyses, and 19 samples in the LOCEAN analyses). This is due to the plastic bottles not
183 been completely proof to air exchange when closed and not frozen.

184



8

185 2.2 Methods

186 $\delta^{18}\text{O}$, $\delta^2\text{H}$ and d-excess will be considered which will be generically addressed as
187 Wisotopes. We aim at a finer scale analysis than in Legrande and Schmidt (2006) where
188 most of the surface North Atlantic is included in one single region. Indeed, this should be
189 viewed as a continuation of Benetti et al (2017)'s regional analysis, as well as water
190 mass analyses such as in Frew et al. (2000) and Voelker et al. (2015), but with only a
191 focus to the surface. We consider sub-regions (Figure 1), in which only samples for
192 which salinity is within specified ranges are retained to avoid the freshest waters on
193 shelves directly influenced by strong local freshwater inputs (rivers, heavy rain, large
194 sea ice melt) which can lead to very skewed salinity distributions (Bingham et al., 2002).

195 The regions are large enough in order to retain data throughout the seasonal cycle, but
196 not too large to correspond to identifiable oceanographic domains with respect to ocean
197 circulation as well as for specific regimes of the water air-sea exchange (Evaporation (E)
198 – Precipitation (P)) and its seasonal cycle or of other freshwater sources. These
199 constraints result in rather large domains in the central subtropical North Atlantic, as
200 well as in the South Atlantic and south-western Indian Ocean, due to poor data coverage.
201 In most of these regions, there is one main source of seawater advected through the
202 region and subject to some freshwater inputs and evaporation resulting in a spatial
203 spread of surface salinity. However, this is not always the case as discussed in Benetti et
204 al. (2017a) for the equatorial region and the eastern subtropical gyre, where upwelling
205 also contributes to the surface water masses in addition to the horizontally advected
206 water. However, Benetti et al (2017a) could not clearly distinguish their respective
207 properties in a (water isotopes, salinity) space.

208 In each region, the data are averaged by month to estimate a seasonal cycle, with
209 unresolved spatial or interannual variability in the sampling contributing to the
210 standard deviation between data. The climatological salinity fields present spatial
211 gradients, which likely also imprint the Wisotopes fields (cf Legrande and Schmidt,
212 2006). With the limited and spatially inhomogeneous sampling, the spatial gradients
213 contribute to a representativeness error on the monthly mean relative to the
214 climatological regional mean. As discussed in App. A, in most regions and for a large part
215 of the seasonal cycle, the spatial standard deviation of climatological monthly salinity



9

216 contributes to a rather large representativeness error which exceeds 0.1 on salinity with
217 the sampling of the CISE-LOCEAN data set. The notable exception is in the better
218 sampled boxes of the North Atlantic subpolar gyre. In some regions, such as in the
219 central Atlantic equatorial box, we also find that for some months with repeated cruises,
220 the average salinity deviates strongly from the box average salinity, most likely due to
221 the spatial sampling, thus inducing large differences in the salinity seasonal cycle.

222 In principle, the better-defined monthly spatial fields of salinity could be used to
223 reconstruct domain-averaged Wisotopes, adopting monthly linear relationships
224 between Wisotopes and S, and assuming that these relationships do not vary
225 interannually. However, Wisotopes data are usually too scarce for estimating a linear
226 relationship on a monthly climatological time scale in individual regions. Thus, to
227 partially circumvent this issue, the compromise adopted here is to group the regional
228 data into four quarters (months 1-3, 4-6, 7-9, 10-12), which, as will be discussed in the
229 results section, often produces too uncertain linear regressions, in which case one
230 resorts to estimate an annual relationship by averaging the linear relationships obtained
231 for each of the four seasons.

232 The linear relationships are obtained by linear regression of Wisotopes as a function of S
233 with least square means in the (S, Wisotopes) space, thus minimizing non-explained
234 residual variance in Wisotopes. To reduce the influence of rare measurements at the
235 lowest or highest salinity as well as outliers, we also estimate a slope and 0-intercept
236 (value of the regression line at $S=0$) by directly fitting the averages of two classes of
237 data, one for the data below and one for the data above the seasonal salinity average.

238 The comparison of the two approaches indicates that the unbiased, but slightly noisier
239 second approach often leads to a larger slope. In the four North Atlantic subpolar gyre
240 boxes, this excess slope averaged ~4%, 6%, 10% of the mean slopes for $\delta^{18}\text{O}$, $\delta^2\text{H}$ and d-
241 excess, respectively, whereas these increases tend to be smaller and less certain in the
242 eastern mid-latitudes and northern tropics. The differences are usually largest for d-
243 excess, and always are within the uncertainty estimates of the slopes in individual
244 regions. Thus, for simplicity, we will only report the second estimate.

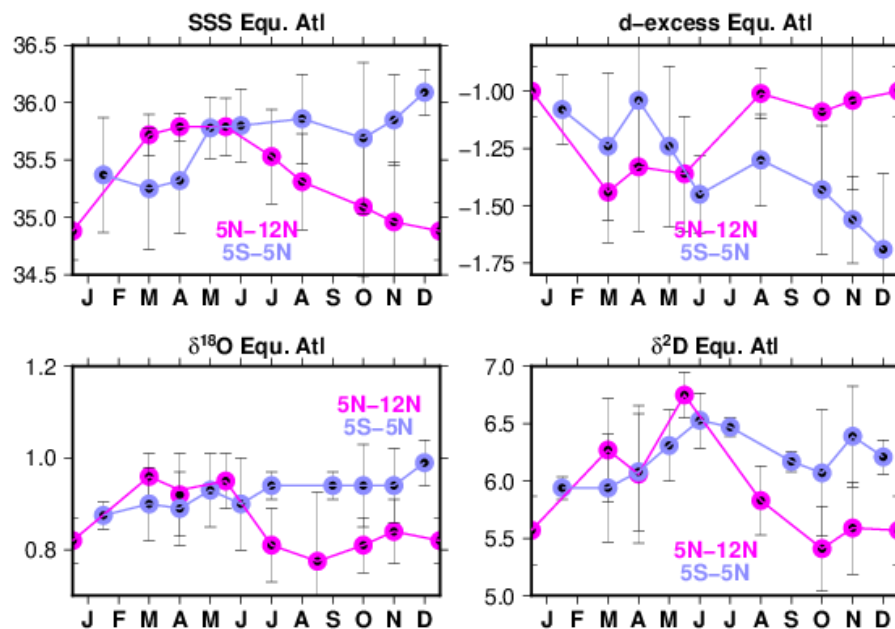
245 3. Results



10

246 3.1 Monthly time series

247 In most regions, monthly standard errors are often large compared to the amplitude of
248 the seasonal cycle. However, there are a few regions where there is sufficient agreement
249 in the salinity seasonal cycle with the climatology, such as the central and western parts
250 of the NASPG, or the central Atlantic north-equatorial (5-12°N). This last region presents
251 a good agreement with salinity climatologies, whereas the equatorial region (5°N-5°S)
252 just to its south presented much less agreement, in part because of large month-to-
253 month spatial differences in the sampling (cf App. A). Thus, we chose to illustrate the
254 average seasonal cycles for surface salinity, $\delta^{18}\text{O}$, $\delta^2\text{H}$ and d-excess in these two
255 contrasting equatorial regions with the monthly means and the standard deviations of
256 the monthly samples (Fig. 2).



257

258 Figure 2: Average seasonal cycle in two central equatorial Atlantic regions for SSS
259 (practical surface salinity, with no unit), $\delta^{18}\text{O}$, $\delta^2\text{H}$ and d-excess (from top to bottom,
260 in ‰). The averages are usually provided monthly, except bi-monthly in a few
261 instances with very insufficient monthly sampling. The standard deviation among
262 the data is plotted (+- 1 standard deviation),



11

263 $\delta^{18}\text{O}$ and $\delta^2\text{H}$ present a variability roughly in phase with SSS in the 5-12°N region, but
264 less so in the 5°N-5°S region (Fig. 2). Furthermore, in each of the two regions, d-
265 excess presents a variability opposite to the one seen in SSS. The two equatorial
266 Atlantic regions are also roughly in phase opposition to each other, at least for SSS
267 and d-excess.

268 In months well sampled, for all variables, the standard error (not presented) is small
269 relative to the amplitude of the seasonal cycle. Typically, for monthly $\delta^{18}\text{O}$ values in
270 the equatorial domain, this estimated standard error varies between 0.01 and
271 0.10‰ (smallest in March and largest in July to September); whereas in January-
272 February, July or August, there are not enough independent data to estimate a
273 standard error. The standard error is typically 6 times larger for monthly $\delta^2\text{H}$ values
274 and 4 times larger for d-excess values than for $\delta^{18}\text{O}$ values. In those two regions it is
275 small enough to resolve a seasonal cycle for all isotopes, albeit not in all months. As
276 mentioned above, for the equatorial region, there is the caveat illustrated on salinity
277 (cf App. A), that part of this apparent seasonal variability is likely associated with
278 seasonal differences in the spatial sampling.

279

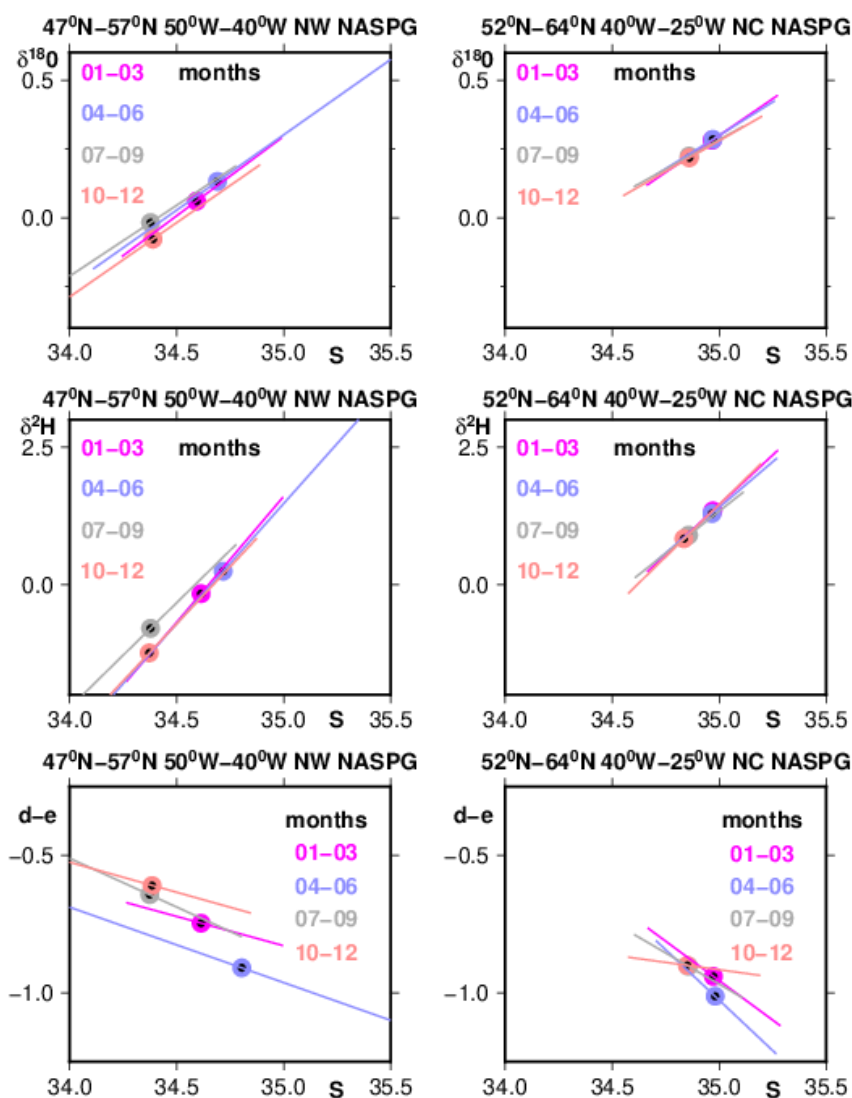
280 3.2 Linear regressions

281 Uncertainties are often large on individual seasonal regressions, in particular when
282 sampling includes less than 10 individual data and for d-excess. This is due to a
283 worse noise/signal ratio for this derived variable, with a smaller proportion of the
284 variability explained by the regression for d-excess. In the particularly well-sampled
285 region south-east of Greenland (Irminger Sea and nearby areas), the residuals of
286 individual data with respect to the linear regression have a standard deviation of
287 0.046, 0.35 and 0.21 ‰ for $\delta^{18}\text{O}$, $\delta^2\text{H}$ and d-excess, respectively (averaged over the
288 four seasons). In this north-central NASPG region, which does not present a large
289 salinity spatial or temporal variability, a significant share of the variance of the
290 individual data in a given season is explained by the mean linear regression to S for
291 $\delta^{18}\text{O}$, $\delta^2\text{H}$ (R^2 of 0.69 and 0.67, averaged over the four seasons, corresponding to
292 correlations which are always significantly different from 0 at $p=0.01$), but not for d-



12

293 excess (R^2 of 0.11). These proportions of course vary from region to region, but for
294 $\delta^{18}\text{O}$, $\delta^2\text{H}$ they decrease towards the lower latitudes (and are as low as 20%-30%
295 near the equator, thus corresponding to correlations which are only significantly
296 different from 0 at $p=0.02$ or 0.05), and for d-excess, they are only high in the
297 equatorial Atlantic domains where the mean regression explains roughly 40% of the
298 variance in individual data (R^2 of 0.40, thus correlations significant at $p=0.01$).



299

300



13

301 Figure 3: Seasonal linear fits of Wisotopes (‰) versus SSS (from top to bottom for $\delta^{18}\text{O}$,
302 $\delta^2\text{H}$ and d-excess) in two regions of the western and central North Atlantic subpolar
303 gyre. Data have only been retained for SSS within 34 to 35.5 and the linear fit is provided
304 within the seasonal SSS range observed. The dots correspond to the averages, with their
305 standard error always within the plotted dots for these two well sampled regions.

306 The seasonal distributions of the linear fits of Wisotopes to SSS is illustrated for two
307 rather well sampled regions in the north-central and western NASPG (Fig. 3). The
308 average salinity cycle roughly corresponds to what is expected in these two regions
309 (Reverdin et al., 2018) with lower summer-fall salinity and larger winter-spring salinity.
310 In both regions the different seasonal distributions for $\delta^{18}\text{O}$, $\delta^2\text{H}$ versus S nearly overlay
311 each other with maybe a small negative isotopic shift in 10-12 contrasting with a
312 positive shift in 7-9, at least for the westernmost region. The latter was attributed to
313 input of sea ice melt to the surface water (Reverdin et al., 2018; Benetti et al., 2016).
314 There are also slightly larger slopes in season JFM, which are attributed to a
315 contribution of depleted brine release for the water samples at the lowest salinities in
316 this season (Benetti et al., 2016).

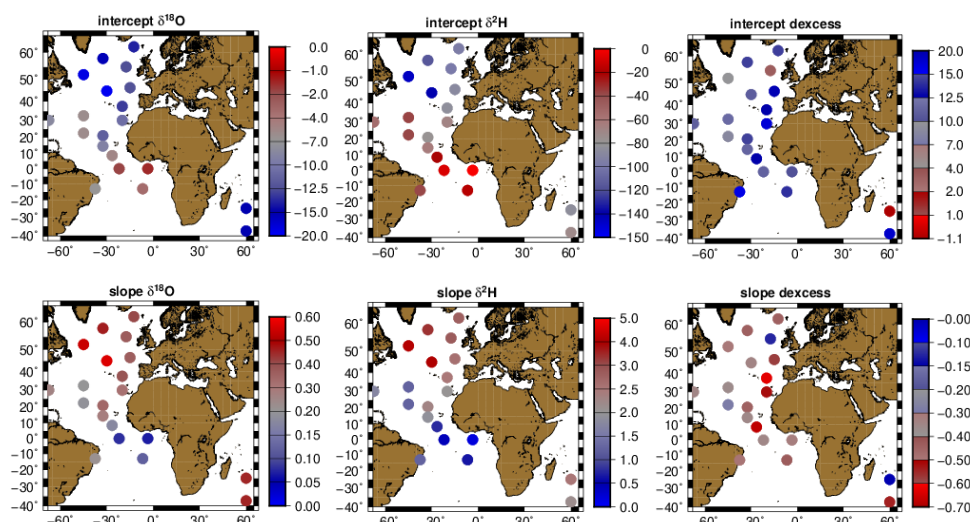
317 The seasonal d-excess versus S distribution also suggests differences according to the
318 seasons, with d-excess apparently shifted to lower values in the spring season. This is
319 also found in another region with reasonable sampling south-east of Iceland. The d-
320 excess deviations across seasons exceed the uncertainty on the averages. For instance,
321 assuming that all data provide independent realizations, the standard errors on the d-
322 excess averages in season 4-6/ 7-9 are respectively 0.04/0.03, and 0.015/0.016‰ for
323 the western and north-central regions of the NASPG, respectively. There is also a
324 suggestion of a weaker slope in season 10-12 with slopes altogether weaker in the
325 western than in the central NASPG region. However, the estimated standard errors for
326 these d-excess versus S seasonal slopes are large and are estimated to be on the order of
327 0.15 ‰/psu in season 10-12 as well as for the other seasons. Thus, even in these well-
328 sampled regions, the differences between seasons in the slope of d-excess versus S
329 linear relationships are within the error bars.

330 3.3 Spatial distribution of linear regressions



14

331 For more than half the regions, the uncertainties on the individual seasonal slopes (and
332 0-intercepts estimated by the extrapolation of the regression line to $S=0$) are larger than
333 between them. To portray the spatial variability in the slopes and 0-intercepts, these
334 seasonal slopes (0-intercepts) are first averaged over the years, retaining only those
335 based on more than 3 individual data.



336

337 Figure 4: Annual averages of the slopes ($\text{‰}/\text{pss}$) and 0-intercepts (‰) of Wisotopes as
338 a function of SSS in the different domains. These annual averages are obtained by
339 averaging the regressions for the 4 seasons, except in the South Indian Ocean, where the
340 data only sample three ($\delta^{18}\text{O}$) or two ($\delta^2\text{H}$ and -excess) seasons. Left for $\delta^{18}\text{O}$, middle for
341 $\delta^2\text{H}$, and right for d-excess (cf table 1 for standard errors on these averages, estimated
342 from the dispersion between the different seasonal averages).

343

344 Table 1: Annual averages of the slopes ($\text{‰}/\text{pss}$) and 0-intercepts (‰) of Wisotopes as a
345 function of SSS in the different domains. These averages (and their standard error in
346 parentheses) are obtained by averaging the regressions for the 4 seasons, except in the
347 South Indian Ocean (last two lines) where they are obtained by averaging only three
348 ($\delta^{18}\text{O}$) or two ($\delta^2\text{H}$ and -excess) seasons, respectively. Left for $\delta^{18}\text{O}$, middle for $\delta^2\text{H}$, and
349 right for d-excess. Regions with large errors usually have at least one season with poor
350 sampling. Slopes and 0-intercepts are willingly reported with more digits than their



15

351 uncertainties, in order to be able to reproduce the linear fit to the distribution of data
 352 (centered on a mean S very different from S=0).

353	Region center	$\delta^{18}\text{O}$		$\delta^2\text{H}$		d-excess	
354		Slope	0-intercept	slope	0-intercept	slope	0-intercept
355	1 45°W/52°N	0.544 (0.013)	-18.77 (0.44)	4.03(0.17)	-146.1 (5.7)	-0.26 (0.04)	8.4 (1.2)
356	2 32°W/58°N	0.473 (0.023)	-16.27 (0.83)	3.45 (0.16)	-119.3 (5.7)	-0.47 (0.13)	15.4 (4.6)
357	3 12°W/62°N	0.409 (0.058)	-14.0 (2.0)	2.87 (0.45)	-98.9 (16.0)	-0.36 (0.07)	11.6 (2.3)
358	4 30°W/45°N	0.579 (0.025)	-20.0 (0.9)	4.24 (0.18)	-147.1 (6.5)	-0.42 (0.14)	13.7 (5.1)
359	5 12°W/55°N	0.386 (0.050)	-13.1 (1.7)	3.09 (0.54)	-106.5 (18.8)	-0.14 (0.10)	3.6 (3.5)
360	6 15°W/47°N	0.354 (0.036)	-11.9 (1.3)	2.57 (0.23)	-87.5 (8.3)	-0.63 (0.24)	21.3 (8.8)
361	7 45°W/32°N	0.199 (0.012)	-6.1 (0.4)	1.21 (0.15)	-36.6 (5.5)	-0.37 (0.09)	11.7 (3.1)
362	8 45°W/22°N	0.196 (0.074)	-6.1 (2.8)	1.27 (0.57)	-39.5 (21.4)	-0.26 (0.32)	7.5 (11.8)
363	9 67°W/30°N	0.270 (0.018)	-8.6 (0.7)	1.82 (0.13)	-58.1 (4.8)	-0.29 (0.16)	9.1 (6.0)
364	10 20°W/37°N	0.385 (0.024)	-13.0 (0.9)	2.45 (0.13)	-83.0 (4.7)	-0.66 (0.20)	22.4 (7.2)
365	11 20°W/30°N	0.328 (0.057)	-11.0 (2.1)	2.13 (0.44)	-71.2 (16.1)	-0.48 (0.08)	16.0 (2.7)
366	12 35°W/21°N	0.339 (0.049)	-11.4 (1.8)	2.29 (0.35)	-77.4 (13.0)	-0.42 (0.08)	13.6 (3.0)
367	13 32°W/14°N	0.275 (0.034)	-9.0 (1.2)	1.87 (0.30)	-61.3 (10.7)	-0.36 (0.09)	11.3 (3.1)
368	14 26°W/8°N	0.194 (0.054)	-6.0 (1.9)	0.79 (0.38)	-22.4 (13.5)	-0.74 (0.17)	25.1 (6.1)
369	15 22°W/0°N	0.073 (0.010)	-1.7 (0.3)	0.38 (0.07)	-7.5 (2.5)	-0.36 (0.03)	11.7 (1.1)
370	16 4°W/0°N	0.061 (0.030)	-1.3 (1.1)	0.18 (0.03)	-0.5 (0.9)	-0.31 (0.06)	9.6 (1.9)
371	17 7°W/13°S	0.119 (0.022)	-3.3 (0.8)	0.62 (0.03)	-16.1 (0.9)	-0.49 (0.02)	16.3 (1.6)
372	18 35°W/13°S	0.223 (0.022)	-7.0 (0.8)	1.27 (0.23)	-39.2 (8.6)	-0.50 (0.07)	16.6 (4.9)
373	19 60°E/25°S	0.481 (0.10)	-16.4 (3.4)	2.45 (0.23)	-82.3 (8.2)	0.00 (0.05)	-1.4 (3.8)
374	20 60°E/37°S	0.442 (0.032)	-5.0 (1.2)	2.17 (1.02)	-72.7 (36.2)	-0.54 (0.20)	18.0 (13.7)
375							

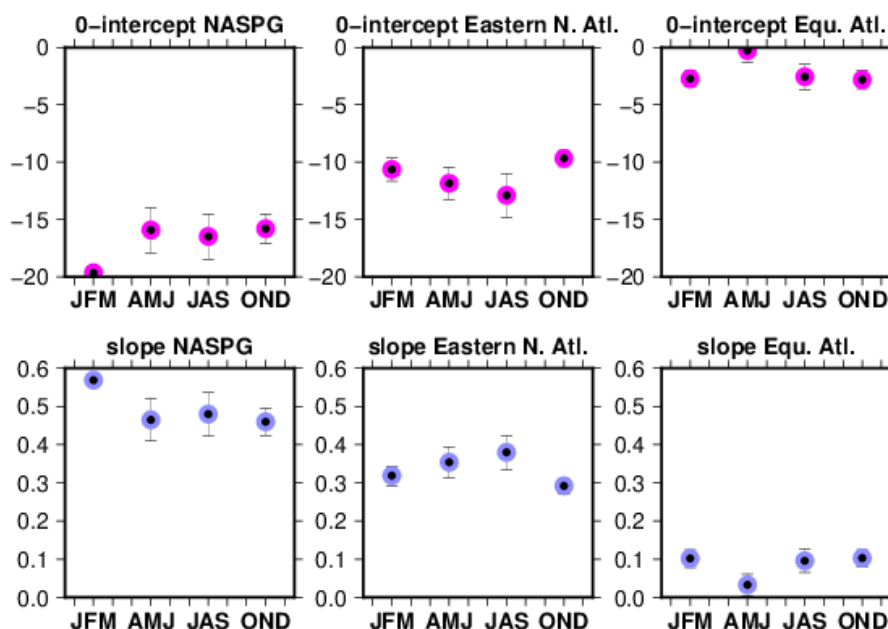
376 The average slopes of $\delta^{18}\text{O}$ and $\delta^2\text{H}$ as a function of SSS (Fig.4, Table 1) are largest in the
 377 northern and western NASPG, as well as South Indian Ocean (for $\delta^{18}\text{O}$), whereas they are
 378 smallest near the equator. Slopes are also smaller in the western subtropical North
 379 Atlantic than in the eastern part. The 0-intercepts follow the patterns of the slope (most
 380 negative in northern NASPG and south Indian Ocean).

381 For d-excess, the pattern is less clear with larger relative errors. Negative slopes are
 382 however largest in the eastern Atlantic (10°N-45°N), as well as in the southern region of
 383 the South Indian Ocean, where it contrasts with weak values further north (but within
 384 the error bars). The d-excess 0-intercepts present a similar pattern (opposite signs),
 385 with large positive 0-intercepts for large negative slope values. The overall anti-
 386 correlation of slope and 0-intercept could be real, but could also arise to some extent
 387 from noise, as SSS=0 is very far from the range of salinity data in which data were
 388 retained, and thus an extrapolation based on a noisy slope estimate would induce an
 389 anti-correlated noise. Clearly the error estimates are large and sampling is insufficient at
 390 least in some of the seasons in a large part of the cases.



391 3.4 Seasonal cycle in the regressions

392 Thus, in order to retrieve a seasonal signature on the slopes and 0-intercepts, one needs
393 to reduce the impact of sampling on the seasonal uncertainties. To do that, we will group
394 regional estimates into larger domains, based on commonality in the sources of water,
395 and whether evaporation dominates over precipitation and other meteoric waters or the
396 opposite. We in particular identify one North Atlantic subpolar gyre domain (4 regions
397 (1 to 4 from Table 1), with usually excess precipitation, a freshwater input from the
398 Arctic and potential contribution of sea ice melt), one east Atlantic domain (from mid-
399 latitudes to northern tropics) (5 regions (6, 10 to 13 from Table 1), with usually excess
400 evaporation and limited local continental Meteoric inputs), and one equatorial and
401 south-equatorial domain (3 regions (15 to 17 from Table 1), with usually excess
402 precipitation, and possible influence of continental Meteoric water). Based on that, we
403 also attempted to create a western subtropical Atlantic domain, and in the eastern
404 Atlantic to separate the northern tropics from the more northern latitudes. However, the
405 uncertainties were then too large in some seasons for these more restricted domains.



406

407 Figure 5: For the larger grouping of regions from table 2), slopes (upper panels, in
408 ‰/psu) and 0-intercepts (lower panel, in ‰) from the regressions of $\delta^{18}\text{O}$ versus SSS



17

409 for the four seasons. From left to right: domain 1 for the North Atlantic Sub-polar gyre, 2
 410 for the eastern North Atlantic, and 3 for the equatorial Atlantic south of 5°N.

411 Table 2: domain-averaged slopes and 0-intersects (standard error in parenthesis) from
 412 the regressions of Wisotope versus SSS for the four seasons (domain 1 for the North
 413 Atlantic Sub-polar gyre, 2 for eastern North Atlantic, and 3 for the equatorial Atlantic
 414 south of 5°N. Seasons 1 to 4 are respectively JFM, AMJ, JAS, and OND. Note that there are
 415 missing season 3 and 4 data in some of the regions and parameters of domain 3). Units
 416 are ‰/pss for all slopes and per mil for all intercepts.

417	Domain season		$\delta^{18}\text{O}$		$\delta^2\text{H}$		d-excess	
418			Slope	0-intercept	slope	0-intercept	slope	0-intercept
419	1	1	0.569 (0.012)	-19.65 (0.45)	4.01 (0.20)	-138.9 (7.0)	-0.35 (0.09)	11.3 (3.8)
420	1	2	0.465 (0.055)	-15.93 (1.95)	3.44 (0.58)	-118.9 (20.5)	-0.54 (0.10)	18.0 (3.4)
421	1	3	0.480 (0.056)	-16.49 (1.98)	3.51 (0.45)	-121.4 (15.7)	-0.32 (0.06)	10.2 (1.9)
422	1	4	0.460 (0.035)	-15.81 (1.27)	3.66 (0.27)	-126.6 (18.8)	-0.24 (0.07)	7.5 (2.4)
423								
424	2	1	0.319 (0.025)	-10.64 (1.00)	2.14 (0.15)	-71.6 (5.5)	-0.47 (0.09)	15.5 (3.6)
425	2	2	0.354 (0.043)	-11.85 (1.50)	2.44 (0.37)	-82.3 (13.0)	-0.47 (0.06)	15.7 (2.3)
426	2	3	0.380 (0.050)	-12.90 (1.90)	2.49 (0.32)	-84.6 (13.5)	-0.55 (0.18)	18.5 (6.5)
427	2	4	0.292 (0.020)	-9.67 (0.70)	1.97 (0.16)	-65.8 (5.5)	-0.54 (0.20)	17.9 (7.4)
428								
429	3	1	0.102 (0.024)	-2.72 (0.84)	0.45 (0.13)	-9.8 (4.3)	-0.35 (0.07)	11.2 (2.9)
430	3	2	0.033 (0.032)	-0.26 (1.00)	0.40 (0.15)	-8.2 (5.5)	-0.45 (0.04)	14.8 (1.9)
431	3	3	0.096 (0.034)	-2.55 (1.12)				
432	3	4	0.103 (0.022)	-2.80 (0.85)	0.28 (0.14)	-4.4 (3.9)		

433 These domain composites (Fig. 5, Table 2) do not show very large/significant seasonal
 434 variability of the slopes/intercepts, but there are some hints of signals. For example, for
 435 the NASPG composite (domain 1, regions 1 to 4 of table 1) for $\delta^{18}\text{O}$, the slope is larger
 436 and intercept more negative in JFM than during the rest of the year, albeit the difference
 437 is barely significant at the 90% confidence level (Fig. 5). On the other hand, table 2
 438 (domain 1) for d-excess indicates a more negative and a larger 0- intercept larger in AMJ
 439 (thus for a different season that the winter deviation reported for $\delta^{18}\text{O}$), but these
 440 differences are not significant at the 90% confidence level.

441 In the equatorial domain (south of 5°N), the slope for $\delta^{18}\text{O}$ is lower and the 0-intercept
 442 less negative in AMJ than during the other seasons, a difference also barely significant at
 443 the 90% confidence level. On the other hand, there is no significant seasonal signal in the
 444 composite for the eastern Atlantic.

445 4. Discussion



18

446 Frew et al (2000) indicate for the NASPG a rather steep slope of the regression line of
447 $\delta^{18}\text{O}$ to salinity (0.59‰/pss) and a rather low 0-intercept (-23‰) indicative of a large
448 contribution of Arctic freshwater origin of the meteoric waters. These values are close
449 but a little larger than the ones we find in the surface waters, but mostly in the western
450 part of the NASPG, and with a smaller uncertainty. The surface data in Voelker et al
451 (2016) a little further south (30-40°N) in the eastern Atlantic indicate a somewhat lower
452 slope (0.32 ‰/pss) and a higher 0-intersect, somewhat similar to what we find in
453 collocated regions 14-16 (similar agreement found for $\delta^2\text{H}$). Benetti et al (2017a) which
454 also includes $\delta^2\text{H}$ and d-excess data show spatial variability in the regression line of
455 isotopes with salinity between some of the same regions of the mid-latitude to
456 equatorial Atlantic that are explored here with a widely extended data set. Benetti et al
457 (2017a) explained to some extent the spatial variability from mid-latitudes to the
458 equator through properties of precipitation and evaporative fluxes, and the relative
459 contribution of the two, with for example the central equatorial areas dominated by
460 precipitations not very depleted in heavy isotopes, thus inducing a small slope in the
461 distributions of $\delta^{18}\text{O}$, $\delta^2\text{H}$, to salinity. None of these earlier papers as well as LeGrande
462 and Schmidt (2006) discuss the seasonal variability in surface data, because the weaker
463 sampling and larger scatter in the earlier datasets would only allow to separate the
464 largest scales (and only for $\delta^{18}\text{O}$).

465 Here, we expanded on these results due to the qualified surface data in the updated
466 CISE-LOCEAN database. To first order, the results we present are coherent with these
467 earlier studies. Sampling remains very low in large areas (Fig. 1), with often too large
468 scatter in the data. There are some regions with large deviations in the regression to
469 salinity: for example, west of the British Isles, the relationships are different possibly
470 because there are multiple sources of freshwater mixing up with North Atlantic drift
471 waters from the subtropics: input from the fresher NASPG waters with an Arctic water
472 input, on one hand, but also less depleted freshwater from rain and runoff from the
473 British Isles. Importantly, this region is poorly sampled, so part of these observations
474 could also be artefacts due to insufficient sampling. Similarly, in the 20-30°S band of the
475 southwestern Indian Ocean, we find some unexpected regressions. Based on Reverdin et
476 al (2025) (and publications therein) this could originate from a combination of two main
477 freshwater sources to this mostly excess-evaporation region, a first one very depleted



19

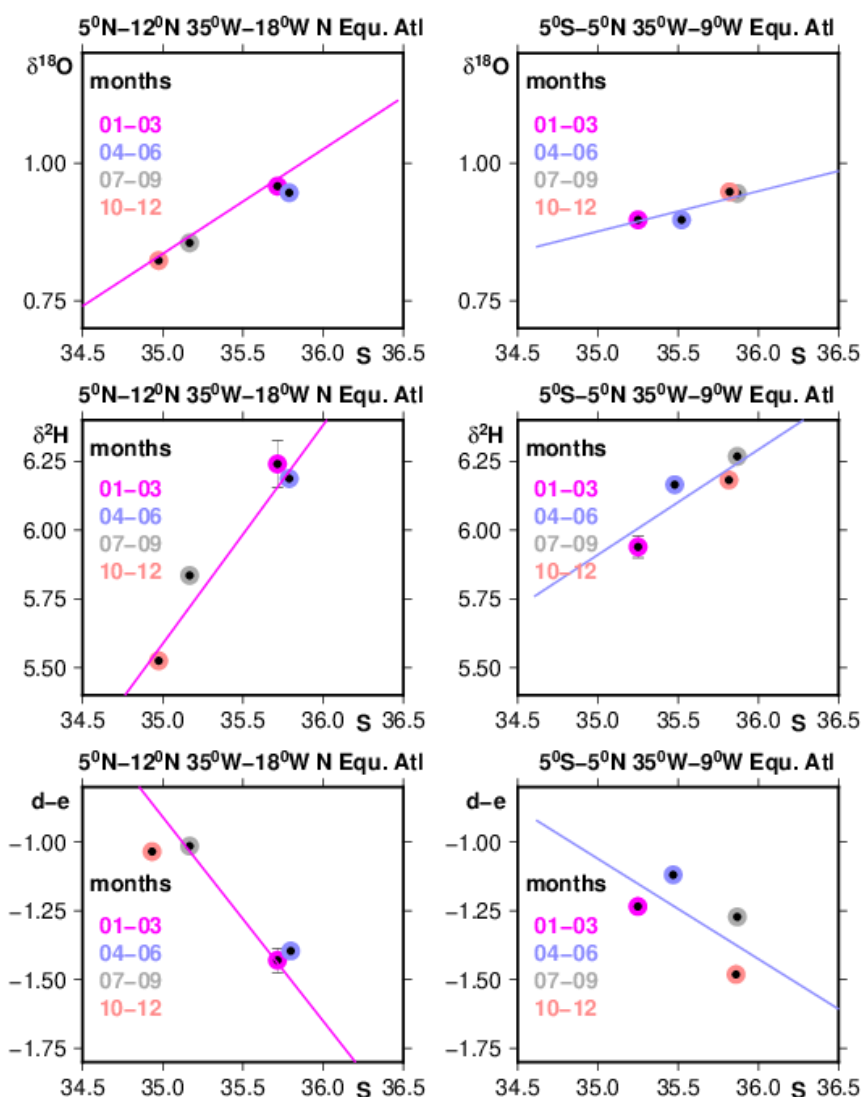
478 which is advected from the surface sub-antarctic austral ocean with southern latitude
479 characteristics, and a second one less depleted carried by the Indo-Pacific throughflow
480 from the western equatorial Pacific and maritime continent to the southwestern tropical
481 Indian Ocean.

482 We also found differences in the linear regressions between the eastern and western
483 tropical/subtropical North Atlantic, albeit sampling in the CISE-LOCEAN database is
484 certainly not very good in the western region. Based on very few data, this was also
485 commented in Benetti et al. (2017a) who interpreted the shift of the distribution to
486 higher $\delta^{18}\text{O}$, $\delta^2\text{H}$ as a likely result of input from western equatorial Atlantic freshwater
487 (in particular from the Amazon-Orinoco discharge and near-equatorial rainfall) in
488 addition to more depleted local freshwater sources. This difference in properties is also
489 confirmed with an analysis of the BATS hydrographic station surface data in the western
490 subtropical North Atlantic.

491 In this study, we examine the seasonal changes in Wisotopes. In the central equatorial
492 Atlantic, when comparing the Wisotopes averages in the 5°N - 12°N region with the ones
493 in the 5°N - 5°S region, we find well defined seasonal cycles in both regions. However,
494 they have very different timings of maxima and minima (Fig. 2). This is expected from
495 the seasonal meridional displacements of the ITCZ and associated changes of ocean
496 circulation and equatorial upwelling, as discussed for SSS (Reverdin et al., 2007; da
497 Allada et al., 2013; Yu et al., 2021). The ITCZ is furthest south in January-March, with a
498 later initiation of the seasonal upwelling at the equator in May, simultaneous with the
499 northward displacement of the ITCZ, as well as the setting of the eastward NECC later on
500 (July-August) bringing water from the Amazon plume in addition to local precipitation
501 to the central equatorial Atlantic further north. This could have induced the higher 0-
502 intercept for $\delta^{18}\text{O}$ and $\delta^2\text{H}$, and the lower intercept for d-excess a signature of Amazon
503 river discharge characteristics in season 10-12 of the 5°N - 12°N domain (For Amazon
504 river properties, cf Benetti et al., 2017a). In each of the two regions, S, $\delta^{18}\text{O}$ and $\delta^2\text{H}$ vary
505 mostly in phase, whereas d-excess varies in opposite phase, consistent with the average
506 regression of these different properties with respect to salinity (Table 1).



20



507

508 Fig. 6: Average linear regressions of Wisotopes (‰) as a function of S (the average of
509 the four seasonal linear regressions) for two central Atlantic equatorial regions (left
510 5°N-12°N; right 5°S-5°N) (from top to bottom for δ¹⁸O, δ²H and d-e); The four average
511 seasonal values are shown.

512 Furthermore, the different seasonal averages for δ¹⁸O and δ²H nearly stand on the
513 average of the seasonal regression lines (Fig. 6). This suggests that the seasonal changes
514 correspond to the action of similar hydrological processes as the spatial spread during



21

515 one season. Notice however that there is a suggestion of a seasonal difference in d-
516 excess with points in seasons April-June and July-September to the right of the average
517 regression line for both regions.

518 In the north-western Atlantic (Fig. 3, but this also holds for nearby regions included in
519 regional grouping 1 of table 2), one finds suggestions of a larger winter regression slope
520 (and more negative 0-intercepts) for $\delta^{18}\text{O}$ and $\delta^2\text{H}$. This is reminiscent of the results in
521 Benetti et al (2016), which they attribute to a contribution of ice formation (brine
522 release), albeit we restrict here the data to salinities above 34, thus possibly missing
523 some of this signal, which is strongest at the lowest salinities. Interestingly, for d-excess,
524 the largest anomaly happens less in winter than in spring, with the average d-excess and
525 individual data shifted to more negative values (at constant S), and with a larger
526 negative slope (at least when averaged over the four s 1 to 4 of Table 1, grouped as
527 domain 1 of Table 2) and a larger positive 0-intercept. It would be tempting to relate
528 that to advection of water affected by sea ice formation processes. However, what is
529 published on sea ice properties during formation at least at equilibrium does not suggest
530 major differences from a ratio of 8 in the fractionation for $\delta^{18}\text{O}$ and $\delta^2\text{H}$ (Souchez et al.,
531 1988), thus inducing no major change for d-excess in the remaining liquid sea water
532 when freezing occurs. Thus, as salinity increases due to brine releases, this would induce
533 a shift of the regression line to the right, thus above on Fig. 3. However, this is the
534 opposite that is observed. As these are areas with active winter mixing and air-sea
535 exchange, although not to the same level in the four regional domains, the changes might
536 also be attributed to those contributions. This would require a modelling approach to
537 fully apprehend.

538

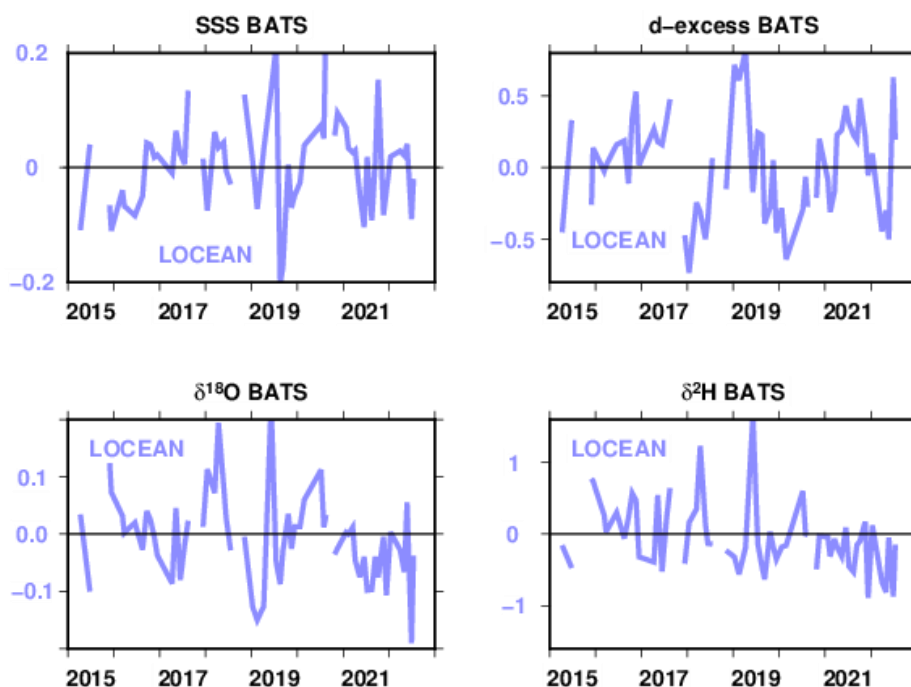
539 However, overall, in most regions investigated, the seasonal differences observed in the
540 regressions to salinity were not found to be significant, even after grouping (averaging)
541 these different regions into larger domains. Thus, the seasonal variability is usually not
542 of a similar magnitude as the large-scale spatial differences. This thus allows for the use
543 of the surface Wisotopes data in comparisons of different databases/sets, even if these
544 datasets have not been collected in the same season (as done in Reverdin et al., 2025).
545 This does not preclude that some areas with large seasonal variability of advection, E



22

546 and P, and different sources of freshwater also present larger seasonal signals in the
547 regional regression lines. This is probably what we observe in the central equatorial
548 Atlantic in the spring-time, and it is also likely the case in areas of the western equatorial
549 Atlantic presenting very large seasonal (and interannual variability) variability, due to
550 the freshwater seasonal discharges originating from the Amazon/Orinoco. This has been
551 observed elsewhere, such as in the western/central equatorial Pacific (Conroy et al.,
552 2017; Horikawa et al., 2023). Higher data density would be required to establish
553 potential seasonal and interannual variability in the regression lines. For example, in the
554 South Indian Ocean, although there is a rather good time series for? austral summer
555 conditions, there are nearly 5 months in the year with no data in the CISE-LOCEAN
556 database.

557 In other areas presented here, there is less evidence for seasonal or interannual
558 variability. In the South Indian Ocean, multi-decadal trends have been described both in
559 the southwestern subtropical region and south of the Subantarctic front, which have
560 been ascribed to changes in the hydrographic cycle and in particular in local evaporation
561 and precipitation (Akhoudas et al, 2023).



562



23

563 Fig. 7: Anomalized time series of SSS (pss), $\delta^{18}\text{O}$, $\delta^2\text{H}$ and d-excess (‰) at BATS
564 (31°50'N, 64°10'W). Only non-flagged LOCEAN data are shown.

565 The BATS site time series in the western North Atlantic subtropics (App. B) is one of the
566 rare sites where there was a concerted effort to regularly gather data over more than 7
567 years. It shows a clear seasonal cycle in S, $\delta^{18}\text{O}$ and $\delta^2\text{H}$, but less so in d-excess, as
568 sampling is still too limited (App. B). Anomalizing the data by subtracting the monthly-
569 averaged seasonal cycle removes a significant part of the variance. However, except for a
570 few peak values reaching 0.2‰ for $\delta^{18}\text{O}$, at times associated with salinity anomalies, the
571 values are usually rather close to the standard errors estimates and the possible
572 magnitudes of systematic errors in the data.

573 Nonetheless, the LOCEAN version of the set suggests higher than normal $\delta^{18}\text{O}$ and $\delta^2\text{H}$ at
574 times in 2016 to 2018 (in particular the winter 2017-2018) and lower values in 2021.
575 These do not seem to correspond to special anomalies in surface salinity. Data of d-
576 excess have an even worse signal over noise ratio, with rms errors in these analyses
577 often exceeding 0.2‰, and further uncertainties associated with poor conservation of
578 some of the samples. They however seem to show a large contrast between the
579 following winters 2017-2018 (negative) and 2018-2019 (positive), as well as the more
580 positive values in 2021. Interpreting these series will require model simulations, in
581 particular to check whether these result from changes in the hydrological cycle or from
582 oceanographic signals, as induced for example by modes of variability such as the North
583 Atlantic Oscillation (NAO, Hurrell et al., 2003), with winter 2017-2018 having a positive
584 NAO index, in contrast to 2021, having a more negative NAO index.

585

586 5. Conclusions

587 Although the current surface data in the CISE-LOCEAN data base mostly collected during
588 the last 25 years, and in particular since 2010, are still in limited number, they offer the
589 possibility to characterize the seasonal cycle of Wisotopes and their relationship to
590 surface salinity in part of the Atlantic Ocean and of the southwestern Indian Ocean. At 0-
591 order in most of these regions, we suggest that the seasonal variations of the regression
592 of Wisotopes to salinity are within the random and representativity errors. There are



24

593 some noticeable seasonal deviations from the mean, in particular in the western North
594 Atlantic subpolar gyre and in the equatorial region. We can better characterize the
595 spatial distribution of this relationship than done before, which hints to small seasonal
596 deviations from the yearly-averaged relationships both for the equatorial Atlantic and in
597 the northwestern subpolar gyre. We also find a weak suggestion of interannual
598 variability at the regularly sampled BATS site in the western subtropical Atlantic.

599 We have not interpreted most of these deviations in a qualitative matter, relating them
600 either to changes in ocean circulation, both horizontal or vertical mixing, or in the water
601 fluxes between the atmosphere, the cryosphere, sea ice, and liquid sea water. In addition
602 to the data, this would require dedicated simulations of forced isotopically-enabled
603 ocean models first validated by the observations (Ayache and Dutay, 2024). In the
604 longer term, this might also require isotopically-enabled earth system models, as the
605 isotopic signatures of these different processes (evaporation, precipitation, continental
606 inputs) evolve in our warming world, as well as the melt of continental glaciers and ice
607 sheets which will imprint on the seawater isotopic composition (Oppo et al., 2007).
608 Additionally, surface seawater isotope data provide model boundary conditions to
609 assess model performance in isotope-enabled Earth system models (e.g. Schmidt et al.,
610 2007; Brady et al., 2019; Cauquoin et al., 2019).

611 The data are still very limited in individual data sets such as the CISE-LOCEAN one, the
612 earlier GISS Global Seawater Oxygen-18 database or the CoralHydro2k Seawater $\delta^{18}\text{O}$
613 Databases. There is an urgent need to put together efforts for better isotopically
614 sampling the near-surface oceans, and thus better constraining processes of the
615 hydrological cycle. This requires active intercomparison of data from different sources,
616 with precise qualification of their differences and respective accuracy. There is hope
617 with ongoing efforts of data retrieval and updating databases that this might be
618 reachable in many parts of the world, despite the obstacles of systematic differences and
619 insufficient data coverage (Reverdin et al., 2025).

620

621 Data availability

622 The CISE-LOCEAN data updated to 2024 are available at

623 <https://www.seanoe.org/data/00600/71186/>.



25

624

625 Author contribution: GR initiated the study and prepared the manuscript with
626 contributions from all coauthors. LG did a first analysis of the seasonal cycles and
627 quality-controlled the CISE-LOCEAN data. HCSL contributed the data from the BATS site,
628 and AV, CW, and HCSL contributed to editing the paper.

629

630 Competing interests: The authors declare that they have no conflict of interest.

631

632 Acknowledgments

633 The LOCEAN isotopic laboratory is supported by 'Observatoire des sciences de l'Univers
634 Ecce Terra' of Sorbonne Université. We are thankful to Catherine Pierre and Jérôme
635 Demange who have set up and help run the facility, and for Aïcha Naamar, Marion
636 Benetti, Camille Akhoudas, and Florine Crossin to have measured some of the water
637 samples. We are grateful for support by INSU, by Claire Lo Monaco and Nicolas Metzl for
638 sampling during the OISO cruises on RV Marion Dufresne, and for the sample collection
639 during the French PIRATA and Ovide repeated cruises. We are also thankful to SNO SSS
640 (Gaël Alory) and the IRD IMAGO team (Denis Diverrès, Stéphane Jacquin, Linn Sekund),
641 for measuring salinity and providing some water from salinity samples, as well as to the
642 more than 100 ship riders on merchant and sailing vessels in the Atlantic Ocean, as well
643 as during hydrographic cruises who collected sea water isotopes samples. We thank the
644 maritime companies EIMSKIP and Royal Arctic Line, for having graciously hosted the
645 ship riders on their vessels, and to have facilitated their work on board. IPSL also
646 repeatedly supported the CISE-LOCEAN database collection and its qualification. The
647 surface salinity climatology is based on 14 years of satellite salinity from product CCI
648 V4.4, and we thank our colleagues Jacqueline Boutin, Anna Parracho and Fabrice
649 Bonjean for their support. This study has been supported by ESA CCI + salinity and CNES
650 SMOS projects. AV also acknowledges financial support by Fundação para a Ciência e a
651 Tecnologia (FCT) through projects Centro de Ciências do Mar do Algarve (CCMAR) basic
652 funding UIDB/04326/2020 (<https://doi.org/10.54499/UIDB/04326/2020>) and
653 programmatic funding UIDP/04326/2020
654 (<https://doi.org/10.54499/UIDP/04326/2020>) and the CIMAR associated laboratory
655 funding LA/P/0101/2020 (<https://doi.org/10.54499/LA/P/0101/2020>).

656



26

657 References

- 658 Akhoudas, C., Sallée, J.-B., Reverdin, G., Haumann, A., Pauthenet, E., Chapman, C. C.,
659 Margirier, F., Lo Monaco, C., Metzl, N., Meilland, J., and Stranne, C.: Isotopic evidence for
660 an intensified hydrological cycle in the Indian sector of the Southern Ocean, *Nature*
661 *Comm.*, <https://doi.org/10.1038/s41467-023-38425-5>, 2022.
- 662 Alory, G., Delcroix, T., Téchiné, P., Diverrès, D., Varillon, D., Cravatte, S., Gouriou, Y.,
663 Grelet, J., Jacquin, S., Kestenare, E., Maes, C., Morrow, R.M., Perrier, J., Reverdin, G.,
664 Roubaud, F.: The French contribution to the Voluntary Observing Ships Network of Sea
665 Surface Salinity, *Deep Sea Res. I*, 105, 1-18, doi:10.1016/j.DSR.2015.08.005, 2015.
- 666 Atwood, A. R., Moore, A.L., Long, S., Pauly, R., DeLong, K., Wagner, A., and Hargreaves, J.A.:
667 The CoralHydro2k Seawater $\delta^{18}\text{O}$ Database, *Past Global Changes Magazine* 32,59, doi:
668 10.22498/pages.32.1.59, 2024.
- 669 Ayache, M., and Dutay, J.-C., Mouchet, A., Tachikawa, K., Risi, C., and Ramstein, G.:
670 Modelling the water isotope distribution in the Mediterranean using a high-resolution
671 oceanic model (NEMO-MED12-watiso v1.0): evaluation of model results against in situ
672 observations, *Geosci. Mod. Develop.*, 17, 6627-6655, [https://doi.org/10.5194/gmd-17-](https://doi.org/10.5194/gmd-17-6627-2024)
673 6627-2024, 2024
- 674 Benetti, M., Reverdin, G., Pierre, C., Khatiwala, S., Tournadre, B., Olafsdottir, S., and
675 Naamar, A.: Variability of sea ice melt and meteoric water input in the surface Labrador
676 Current off Newfoundland, *J. Geophys. Res. Oceans*, 121(4), 2841–2855, 2016.
- 677 Benetti, M., Reverdin, G., Aloisi, G., and Sveinbjörnsdóttir, A.: Stable isotopes in surface
678 waters of the Atlantic Ocean: indicators of ocean-atmosphere water fluxes and oceanic
679 mixing processes, *J. Geophys. Res. Oceans*, 122, doi:10.1002/2017JC012712, 2017a.
- 680 Benetti, M., Sveinbjörnsdóttir, A. E., Ólafsdóttir, R., Leng, M. J., Arrowsmith, C., Debondt,
681 K., Fripiat, F., and Aloisi, G.: Inter-comparison of salt effect correction for $\delta^{18}\text{O}$ and $\delta^2\text{H}$
682 measurements in seawater by CRDS and IRMS using the gas-H₂O equilibration method,
683 *Marine chemistry*, doi:10.1016/j.marchem.2017.05.010, 2017b.
- 684 Bingham, F. M., Howden, S. D., and Koblinsky, C. J.: Sea surface salinity measurements in
685 the historical database, *J. Geophys. Res. Oceans*, 107, 10.1029/2000JC000767, 2002.
- 686 Boutin, J., Chao, Y., Asher, W. E., Delcroix, T., Drucker, D., et al.: Satellite and In Situ
687 Salinity: Understanding Near-Surface Stratification and Subfootprint Variability, *Bull. of*
688 *the Amer. Meteor. Soc.*, 97 (8), pp.1391-1407. 10.1175/BAMS-D-15-00032.1, 2016.



- 689 Boutin, J., Reul, N., Koehler, J., Martin, A., Catany, E., Guimbard, S., Rouffi, F., Vergely, J.-L.,
690 Arias, M., Chakroun, M., Corato, G., Estella-Perez, V., Hasson, A., Josey, S., Khvorostyanov,
691 D., Kolodziejczyk, N., Mignot, J., Olivier, L., Reverdin, G., Stammer, D., et al: Satellite-Based
692 Sea Surface Salinity Designed for Ocean and Climate Studies, *J. Geophys. Res. Oceans*,
693 126, 11, <https://doi.org/10.1029/2021JC017676>, 2021.
- 694 Brady, E., Stevenson, S., Bailey, D., Liu, Z., Noone, D., Nusbaumer, J., Otto-Bliesner, B. L.,
695 Tabor, C., Thomas, R., Wong, T., Zhang, J., Zhu, J.: The connected isotopic water cycle in
696 the Community Earth System Model Version 1, *J. Adv. Model. Earth Syst.*, 11, 8,
697 <https://doi.org/10.1029/2019MS001663>, 2019.
- 698 Cauquoin, A., Werner, M., Lohmann, G.: Water isotopes – climate relationships for the
699 mid-holocene and preindustrial period simulated with an isotope-enabled version of
700 MPI-ESM, *Clim. Past* 15, 1913-1937, <https://doi.org/10.5194/cp-15-1913-2019>, 2019.
- 701 Conroy, J. L., Thompson, D. M., Cobb, K. M., Noone, D., Rea, S., and LeGrande, A. N.:
702 Spatiotemporal variability in the $\delta^{18}\text{O}$ -salinity relationship of seawater across the
703 tropical Pacific, *Paleoceanography*, 32, 484–497,
704 <https://doi.org/10.1002/2016PA003073>, 2017.
- 705 Da-Allada, C. Y., Alory, G., du Penhoat, Y., Kestenare, E., Durand, F., and Hounkonnou, N.
706 M.: Seasonal mixed-layer salinity balance in the tropical Atlantic Ocean: mean state and
707 seasonal cycle, *J. Geophys. Res. Oceans*, 118, 332-345 ISSN 0148-0227,
708 <https://doi.org/10.1029/2012JC008357>, 2013.
- 709 Frew, R. D., Dennis, P. F., Heywood, K. J., Meredith, M. P., and Boswell, S. M.: The oxygen
710 isotope composition of water masses in the northern North Atlantic, *Deep-Sea Res. I*, 47,
711 2265-2286, 2000.
- 712 Glaubke, R. H., Wagner, A., and Sikes, E. L.: Characterizing the stable oxygen isotopic
713 composition of the southeast Indian Ocean, *Mar. Chem.*, 262, 177–185,
714 <https://doi.org/10.1016/j.marchem.2024.104397>, 2024.
- 715 Hennig, A., Mucciarone, D. A., Jacobs, S. S., Mortlock, R. A., and Dunbar, R. B.: Meteoric
716 water and glacial meltwater in the southeastern Amundsen Sea: a time series from 1994
717 to 2020, *The cryosphere*, 18, 791-818, <https://doi.org/10.5194/tc-18-791-2024>, 2024.
- 718 Hilaire-Marcel, C., Kim, S. T., Landais, A., Ghosh, P., Assonov, S., Lécuyer, C., Blanchard, M.,
719 Meijer, H. A., and Steen-Larsen, H. C.: A stable isotope toolbox for water and inorganic
720 carbon cycle studies, *Nature Reviews Earth & Environment* 2 (10), 699-719, 2021.



28

- 721 Horikawa, K., Kodaira, T., Zhang, J., and Obata, H.: Salinity-oxygen isotope relationship
722 during an El Niño (2014-2015) in the southwestern Pacific and comparisons with
723 GEOSECS data (La Niña, 1973-1974), *J. Mar. Chem.*, 249,
724 <https://doi.org/10.1016/j.marchem.2023.104222>, 2023.
- 725 Hurrell, J. W., Kushnir, Y., Ottersen, G., and Visbeck, M.: An overview of the North Atlantic
726 Oscillation. Edited by: J.W. Hurrell, Y. Kushnir, G. Ottersen and M. Visbeck, *Geophys.*
727 *Monog. Ser.*, 134, 35 pp, <https://doi.org/10.1029/134GM01>, 2005.
- 728 Konecky, B. L. et al.: The Iso2k database: a global compilation of paleo- $\delta^{18}\text{O}$ and $\delta^2\text{H}$
729 records to aid understanding of Common Era climate, *Earth Syst. Sci. Data*, 12, 2261–
730 2288, <https://doi.org/10.5194/essd-12-2261-2020>, 2020.
- 731 LeGrande, A. N. and Schmidt, G. A.: Global gridded data set of the oxygen isotopic
732 composition in seawater, *Geophys. Res. Lett.* 33,
733 <https://doi.org/10.1029/2006gl026011>, 2006.
- 734 Oppo, D. W., Schmidt, G. A., and LeGrande, A. N.: Seawater isotope constraints on tropical
735 hydrology during the Holocene, *Geophys. Res. Lett.* 34, L13701,
736 <https://doi.org/10.1029/2007GL030017>, 2007.
- 737 Phillips, H. E., and Joyce, T. M.: Bermuda's tale of two time series: Hydrostation S and
738 BATS, *J. Phys. Oceanogr.*, 37, 554-571, <https://doi.org/10.1175/JPO2997.1>, 2007.
- 739 Reverdin, G., Kestenare, E., Frankignoul, C., and Delcroix, T.: In situ surface salinity in the
740 tropical and subtropical Atlantic Ocean. Part I. Large scale variability, *Progress in Oceanogr.*,
741 73, 3, 311-340, <https://doi.org/10.1016/j.pocean.2006.11.004>, 2007.
- 742 Reverdin, G., Metzl, N., Olafsdottir, S., Racapé, V., Takahashi, T., Benetti, M., Valdimarsson,
743 H., Benoit-Cattin, A., Danielsen, M., Fin, J., Naamar, A., Pierrot, D., Sullivan, K., Bringas, F.,
744 and Goni, G., SURATLANT: a 1993-2017 surface sampling in the central part of the North
745 Atlantic subpolar gyre, *Earth Sci. Sys. Data*, 10, 1901-1924,
746 <https://doi.org/10.5194/essd-10-1901-2018>, 2018.
- 747 Reverdin, G., et al.: The CISE-LOCEAN sea water isotopic database (1998-2021), *Earth*
748 *Sci. Sys. Data*, <https://doi.org/10.5194/essd-2022-34>, 2022.
- 749 Reverdin, G., Waelbroeck, C. Voelker, A. H., and Meyer, G.: Technical note: Large offsets
750 between different datasets of seawater isotopic composition: an illustration of the need
751 to reinforce intercalibration efforts, *Ocean Sci.*, 21, 567-575,
752 <https://doi.org/10.5194/os-21-567-2025>, 2025.



29

753 Schmidt, G. A., LeGrande, A. N., and Hoffmann, G.: Water isotope expressions of intrinsic
754 and forced variability in a coupled ocean-atmosphere model, *J. Geophys. Res.* 112,
755 D10103, <https://doi.org/10.1029/2006jd007781>, 2007.

756 Steen-Larsen, H.-C., and Zannoni, D.: A versatile water vapor generation module for
757 vapor isotope calibration and liquid isotope measurements, *Atmos. Measur. Tech.*, 17,
758 14, <https://amt.copernicus.org/articles/17/4391/2024/2024>, 2024.

759 Voelker, A., Colman, A., Olack, G., Waniek, J. J., and Hodell, D.: Oxygen and hydrogen
760 isotope signatures of Northeast Atlantic water masses, *Deep-Sea Res. II*, 116, 89-106.
761 <https://doi.org/10.1016/j.dsr2.2014.11.006>, 2015.

762 Yu, L., Bingham, F. M., Dinnat, E. P., Fournier, S., Melnichenko, O., Tang, W., and Yueh, S.
763 H.: Revisiting the global patterns of seasonal cycle in sea surface salinity, *J. Geophys. Res.*
764 *Oceans*, 126, <https://doi.org/10.1029/2020JC016789>, 2021.

765



766 Appendix A : Comparison of salinity box averages

767 We compare the box averages salinity seasonal cycle estimated from the LOCEAN data
768 to climatological monthly fields of in situ salinity from Reverdin et al. (2007) updated to
769 1977-2016 and from the satellite-based CCI V4.4 SSS product averaged over 2011-2024
770 (Boutin et al., 2021). These two climatologies provide information on the effect of the
771 limited spatial sampling in the boxes on the monthly box averages. The results with
772 these two climatologies which differently span most of the period in which data were
773 collected are rather similar. In most regions and for a large part of the seasonal cycle, we
774 find that the spatial standard deviation of climatological monthly salinity contributes to
775 a rather large representativeness error with the sampling of the LOCEAN data set which
776 exceeds 0.1 on salinity for most months and regions. The notable exception is in the
777 better sampled boxes of the North Atlantic subpolar gyre.

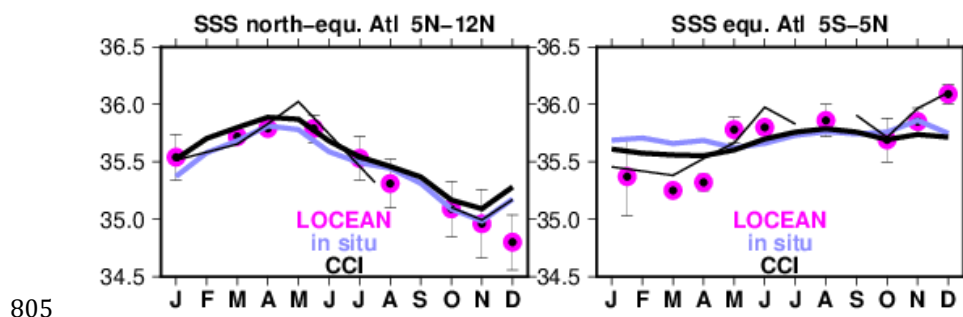
778 For example, in the central Atlantic north-equatorial (5-12°N) and equatorial (5°N-5°S)
779 domains, the spatial standard deviation of climatological monthly salinity in the in-situ
780 climatology varies between 0.2 (north-equatorial in months 1-4) to 0.4 (north-
781 equatorial, months 6-11) or even 0.5 (equatorial, months 10-11-12-1), and this both for
782 the in situ and the CCI climatologies. Assuming random spatial sampling in the current
783 LOCEAN dataset, this would contribute to a representativeness error which exceeds 0.1
784 on salinity for most months.

785 However, there are other contributions to the standard error on the monthly averages,
786 as a large proportion of the data can originate from a single cruise, and all data are not
787 independent with respect to interannual, higher frequencies than monthly or spatial
788 variability within the domain. These all contribute to the difference of S to the average
789 climatological seasonal cycle. In the instance of the North Equatorial region on Fig. 2
790 (and other regions too), the LOCEAN S seasonal cycle is more irregular than in the
791 climatologies, but the differences are usually less than σ the standard deviation between
792 all the data. They are however larger than if one assumes that all data are independent
793 random representation of the mean (thus with a standard error σ/\sqrt{n}). The
794 compromise we adopt to estimate the standard error is to use as the number of degrees
795 of freedom $n/2$. We also propagate that estimate to the other parameters (Wisotopes),
796 assuming that what is found for S is a model for the sampling issues.



31

797 Even, with that assumption, we find in regions which are irregularly spatially sampled
798 that the differences in SSS with climatologies are larger than the estimated standard
799 error. Part of that is associated with spatial variability of the poorly sampled mean
800 monthly fields, as seen for the central equatorial Atlantic region 5°S-5°N (Fig. 2), when
801 comparing the CCI climatology averaged spatially over the box (thick black line) with the
802 climatology sampled at the position of the data (thin black line). The thin black line
803 there, but also to a lesser extent for the north equatorial box (5°N-12°N) is closer to the
804 monthly data average, with differences compatible with the standard error estimates.



806 Figure A1: Comparison of average seasonal cycle in the LOCEAN data set (dots with
807 error bars) with two climatologies (curves), the blue one for 1977-2016 (In situ;
808 Reverdin et al., 2007), and the black ones being for the CCI V4.4 SSS for 2010-2023
809 (Boutin et al., 2021) (the thick curve for the box averages, and the thin curve for the
810 average at the positions of the sampling). The standard errors plotted on the LOCEAN
811 monthly averages, are estimated taking $n/2$ as the number of degrees of freedom, where
812 n is the sample size.

813



32

814 Appendix B: BATS seasonal variability

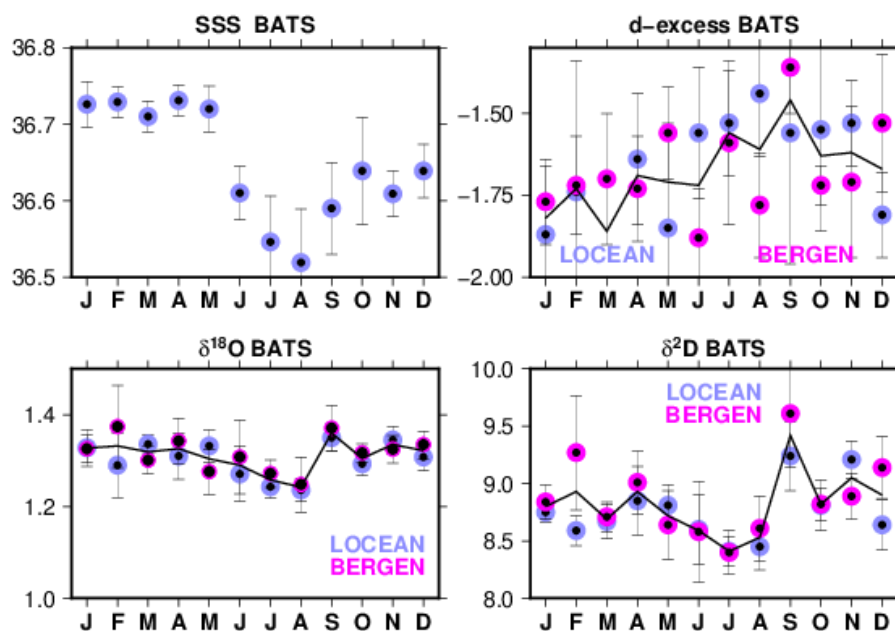
815

816 Water samples were collected nearly monthly from 2015 to 2022 at the BATS
817 hydrographic site in the western subtropical Atlantic (close to (31°50'N, 64°10'W)).
818 They were stored in plastic bottles which were frozen once returning to the Bermuda
819 oceanographic station. They were later unfrozen in Bergen and run in three separate
820 days on a Picarro CRDS L2130. Then, the samples were refrozen, and were unfrozen
821 again shortly before been shipped to LOCEAN, where they were kept unfrozen at 4°C,
822 before analysis (thus, for some, up to nearly two months).

823 The BATS data have been validated and flagged as usually done at LOCEAN, based on
824 anomalous d-excess and compared to the set analyzed at the Univ. Bergen (referred to
825 as Bergen, later on). Out of 80 samples, some were flagged as likely bad when d-excess
826 was deemed too low (6 for the Bergen set; 15 for the LOCEAN time series) and some as
827 likely good but suspicious if d-excess as too high (2 for Bergen, 5 for LOCEAN). Five out
828 of the six likely bad flagged data in Bergen were also flagged as such in the LOCEAN data
829 set, but not the two Bergen data flagged as suspicious. The larger number of flagged data
830 at LOCEAN suggests that the plastic bottles in which the samples were stored exchanged
831 water molecules with the outside air, after been unfrozen for shipment to LOCEAN and
832 before analysis. The number of suspicious flags (d-excess deviating by up to +1 ‰ from
833 usual) as well as the non-consistency for that between the two sets is suggestive of some
834 noise in the analyses. In particular, during the daily runs in December 2025/January
835 2026 there often was poor reproducibility of a reference sample in the runs. However,
836 based on replicates, we expect that standard errors on the LOCEAN measurements is
837 usually less than 0.05‰.



33



838

839 Figure B1. Monthly-averaged seasonal cycle at BATS of SSS, $\delta^{18}\text{O}$, $\delta^2\text{H}$ and d-excess
840 (from top to bottom, in ‰) (averages and standard errors). The two colours correspond
841 to the LOCEAN and Bergen analyses of the samples, and the thin line is the average of
842 the two sets.

843 We also suspect systematic shifts in the Bergen set between three different days of
844 analysis. We thus adjusted the Bergen set to the LOCEAN set by comparing unflagged
845 data separately for each of the three days of analysis in Bergen. After that, both sets are
846 used to estimate an average seasonal cycle (Fig. B1). Because of the small sample size
847 (averaging on the order of 5-6 in each calendar month), the standard errors are large.
848 The two sets of analyses indicate a rather coherent variability in S, $\delta^{18}\text{O}$ and $\delta^2\text{H}$ with
849 differences within standard error bars (a mostly similar cycle is also found in the Bergen
850 set prior to the adjustment). There are hints of a seasonal cycle with lowest S in June to
851 September. The summer minimum is a prominent feature in the longer BATS time
852 series, although in 1990-2000, it shows the minimum in September (Phillips and Joyce,
853 2007). Fig. B1 also shows lower $\delta^{18}\text{O}$ and $\delta^2\text{H}$ in June-August. Because of the limited
854 sampling and the standard error bars, the large increase of $\delta^{18}\text{O}$ and $\delta^2\text{H}$ in September,
855 with no counterpart in S, may not be a representative feature of an average seasonal



34

856 cycle. However, it is tempting to associate it with the beginning of the tropical storm
857 season in late summer, and possible individual storm signatures. Because of the
858 standard error bars in both analyses, we attribute better confidence in the average of
859 the two sets of analyses (shown as the thin black line in Fig. B1), with overall a
860 variability in $\delta^{18}O$ nearly following the spatial relation between $\delta^{18}O$ and $\delta^{13}C$
861 in this region, except for September (region 9 of Table 1).

862 The standard errors are large on the $\delta^{18}O$ -excess monthly averages. However, the average
863 of the two sets suggests a seasonal cycle with lower $\delta^{18}O$ -excess in Dec.-May, and higher in
864 Jul-Nov..

865